Dalton Transactions **2017**, *46*, 16439-16445

https://doi.org/10.1039/C7DT03915H

Dalton Transactions

ARTICLE

Redox Non-Innocent Bis(2,6-diimine-pyridine) Ligand-Iron Complexes as Anolytes for Flow Battery Applications

Received 00th January 20xx,
Accepted 00th January 20xx

DOI: 10.1039/x0xx00000x

www.rsc.org/

Gabriel Martins da Silva Almeida Duarte†, Jason D. Braun†, Patrick K. Giesbrecht and David E. Herbert*

Diiminepyridines are a well-known class of "non-innocent" ligands that confer additional redox activity to coordination complexes beyond metal-centred oxidation/reduction. Here, we demonstrate that metal coordination complexes (MCCs) of diiminepyridine (DIP) ligands with iron are suitable anolytes for redox-flow battery applications, with enhanced capacitance and stability compared with bipyridine analogs, and access to storage of up to 1.6 electron equivalents. Substitution of the ligand is shown to be a key factor in the cycling stability and performance of MCCs based on DIP ligands, opening the door to further optimization.

Introduction

The increasing share of energy generation being devoted to renewable but intermittent sources such as solar, hydroelectric and wind has led to a resurgence of interest in flow batteries for scalable, inexpensive energy storage.[1] In redox flow batteries (RFBs), electrical energy is converted to chemical energy through electrochemical interconversion of a redox pair acting as the electrolyte, which in contrast to conventional batteries, are spatially separated from the electrode.[2] If both the oxidized and reduced forms of the pairs are stable, RFBs offer promising options for long-term storage, where scalability in part will ultimately depend on the scarcity or abundance of the materials used as catholyte/anolyte.[3] Metal coordination complexes (MCCs) that can exhibit one or more accessible redox couples are commonly used in aqueous RFBs.[4] Water, however, exhibits a low voltage window (~ 1.5 V), limiting its overall energy storage capacity and compatibility with alternative MCCs.[5] In employing an organic solvent such as acetonitrile with a larger voltage window (5.0 V), the challenge is to synthesize MCCs that can undergo multiple reversible electron transfers that occur past the water voltage window and are highly soluble in all oxidized and reduced forms. From this, a higher RFB energy storage capacity can be achieved, with a higher energy density output.[6]

Redox 'non-innocent' ligands are often paired with base metals in catalysis to allow earth-abundant first row transition metals to access multi-electron redox reactions unachievable for the metal itself.[7] In such complexes, the ligand is the site of oxidation/reduction, avoiding unfavourable electronic configurations at the metal centre, but also enabling the coordination complex to engage in additional redox events both at the ligand and the metal. Coordination complexes of 'non-innocent' ligands can thus confer additional performance to abundant metals in RFBs.[8] We set out to explore the applicability of the prototypical redox non-innocent (2,6-diimine)pyridine[9] scaffold (DIP, Figure 1) as a ligand in an MCC anolyte for RFBs. DIP ligands have been shown to act as electron reservoirs able to accommodate up to three additional electrons, and triply reduced DIP ligands have been identified in s-,[10a] f-[10b] and d-block[10c] metal complexes.

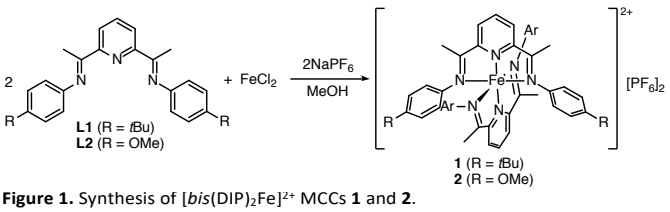

Figure 1. Synthesis of [*bis*(DIP)$_2$Fe]$^{2+}$ MCCs **1** and **2**.

In particular, we examined two DIP proligands, differing in the presence of *tert*-butyl (**L1**) or methoxy substitutents (**L2**) in the 4-positions of the imine-based aryl rings, and their octahedral [*bis*(DIP)$_2$Fe]$^{2+}$ coordination complexes. While the use of organometallic iron complexes[11] and iron coordination complexes[12] has been demonstrated in aqueous and non-aqueous RFBs, the integration of redox-active ligands with the base metal iron has been considerably less explored.[5, 6b, 13] Octahedral ligand environments for each iron supported by two DIP ligands were targeted to reduce ligand dissociation, with tridentate chelation anticipated to impart greater

[a] Department of Chemistry and the Manitoba Institute for Materials
University of Manitoba
144 Dysart Road, Winnipeg, Manitoba, R3T 2N2, Canada
*E-mail: david.herbert@umanitoba.ca

† These authors contributed equally to this work.

Electronic Supplementary Information (ESI) available: additional experimental details, supporting figures and tables, multinuclear NMR, CIF, UV-Vis spectra, and additional electrochemical plots. See DOI: 10.1039/x0xx00000x

complex stability and higher cyclability compared with bidentate redox non-innocent ligand candidates such as diimines[14] or bipyridines.[13a, 15] 2,6-unsubstituted arenes were chosen as substituents at nitrogen to reduce steric congestion about the metal centre, as bulkier DIP ligands can induce ligand hemilability in reduced, octahedral *bis*(DIP)$_2$Fe complexes.[16]

Results and Discussion

Synthesis and Characterization of Coordination Complexes

Coordination complex **1** and the previously reported **2**[17] were prepared with hexafluorophosphate $[PF_6]^-$ counterions by reacting their respective proligands with $FeCl_2$ in methanol under an inert atmosphere to form dark purple solutions. An excess of solid $NaPF_6$ was then added to provide non-coordinating counterions in common with the added electrolyte (nBu$_4$PF$_6$). The MCCs show good solubility in polar organic solvents (solubility of **1** > 0.13 M; **2** > 0.26 M in CH_3CN) and were precipitated from dichloromethane (DCM) into pentane to give **1** and **2** as air and moisture-stable, deep purple solids in yields > 90%. Complexes **1** and **2** were fully characterized in solution by multinuclear NMR, UV-Vis and Mössbauer spectroscopy, with spectroscopic data for **2** compared to the literature.[17] Mössbauer spectroscopic parameters for **1** are very close to those reported for **2**[17] (Table 1, Figure S19), with both isomer shifts and quadrupole splitting parameters consistent with low-spin Fe (II), and in line with parameters for related DIP supported Fe(II) centres.[16-18]

Table 1. Redox and Mössbauer parameters for **1** and **2**[17]

Compound	$E_{1/2}$/V	Δ_{ptp}/mV	i_{red}/i_{ox}	δ/mms^{-1}	Δ/ mms^{-1}
1	-1.32	60	0.95	0.2237(6)[a]	1.002(1)[a]
	-1.59	60	1.04		
	0.90	69	0.97		
2[17]	-1.30	61	0.99	0.235(8)[b]	1.081(5)[b]
	-1.60	75	0.97		
	0.86	77	0.97		

[a] Measured at 10 K. [b] Measured at 80 K; from reference [17].

To confirm an octahedral *bis*(DIP)$_2$ ligand environment, the solid-state structure of **1**$[PF_6]_2$ was determined by single-crystal X-ray diffraction (XRD). A representation of the cation of **1** is shown in Figure 2a, and pertinent bond distances and angles for both **1** and **2**[17] included in Table 2. In the solid-state, the two neutral, tridentate ligands are bound to iron in a meridional fashion, with the pyridine nitrogens *trans* to each other [N_{pyr}-Fe-N_{pyr} 179.44(11)°]. The Fe atom sits at the centre of a distorted octahedron, evidenced by N_{imine}-Fe-N_{imine} bond angles of ~160° for each ligand. This bond angle is nearly identical to those reported for sterically unencumbered, four-coordinate Fe(II) structures containing only a single DIP ligand, indicating that packing two DIP ligands around a single Fe atom does not introduce significant strain. When compared with the structure of **2**,[17] incorporation of a bulkier *tert*-butyl aromatic substituent does not significantly influence the geometry around the Fe metal centre, consistent with their distant placement on the flanking *N*-phenyl rings.

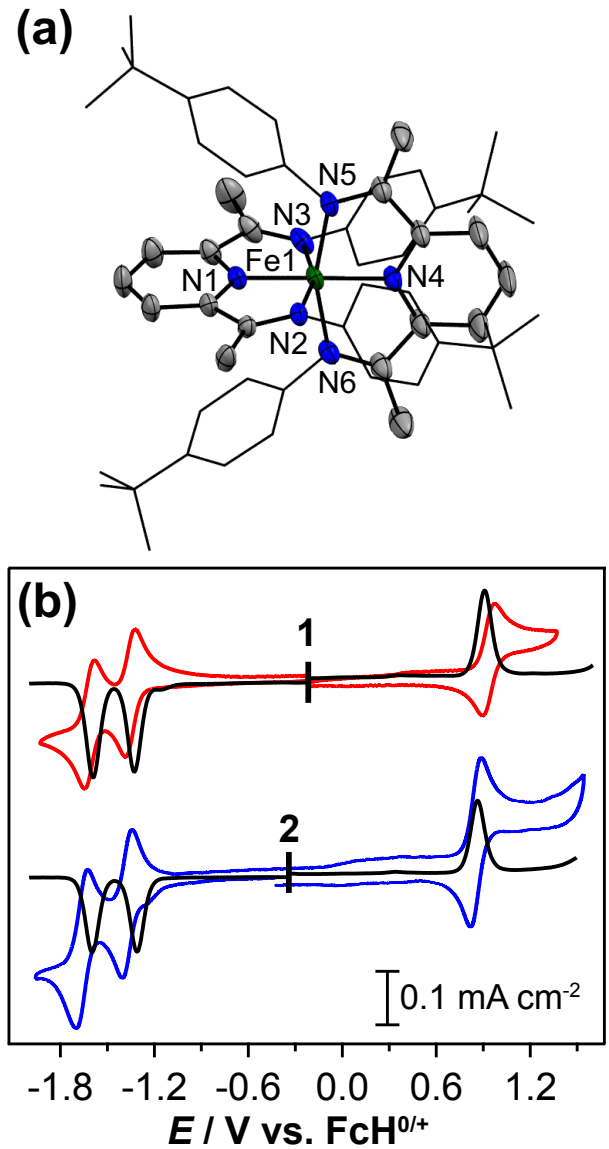

Figure 2. (a) ORTEP of **1**$[PF_6]_2$ with thermal ellipsoids shown at a 50% probability level, solvent molecules, counterions and hydrogen atoms are omitted for clarity; (b) CV/DPVs of **1** and **2** (0.6 mM of analyte, 0.1 M nBu$_4$PF$_6$ in acetonitrile, GCE, scan rate = 100 mV/s).

Cyclic voltammetry (CV) and differential pulse voltammetry (DPV) analysis of **1** and **2** revealed nearly identical redox behaviour for both MCCs, with two reversible 1e$^-$ reductions evident at -1.3 V and -1.6 V, and one 1e$^-$ oxidation observed near +0.8 V vs. FcH$^{0/+}$ (Figure 2b). The cathodic events are assigned as ligand-centred based on previous analysis of the redox behaviour of DIP complexes of Fe.[10c, 16-17] The oxidation peak is similarly assigned to a metal-centred oxidation process (Fe^{2+}/Fe^{3+}). Spectroelectrochemical oxidation of **1** ($E_{applied}$ = -0.2 to 2.3 V; Figure 3a) shows conversion to a single new complex with clear isosbestic points corresponding to the reversible 1e$^-$ redox couple observed by CV at +0.8 V. Bulk reduction of **1** in a spectroelectrochemical cell ($E_{applied}$ = -0.2 to

-1.4 V) showed less well-defined isosbestic points (Figure 3b), but the appearance of a shoulder at ~ 800 nm is in line with previously reported spectra for electrochemically reduced **2**,[17] and the appearance of a low energy band at 1420 nm is consistent with reduction to a single ligand-based radical.[19]

With respect to electrical energy storage, multiple electron transfers by a single complex offers the possibility of high storage capacity.[6b] Furthermore, the potentials of the redox events demonstrated by the MCCs **1** and **2** surpass the voltage limits of water (ca. -1.2 V vs. $FcH^{0/+}$).[20] The two reduction events for both **1** and **2** are highly reversible by CV (Table 1). In particular, both show peak current ratios of close to unity and narrow peak separations, with a slightly larger separation (still close to the Nerstian limit 59 mV) separation for the second reduction event.[21] We therefore proceeded to examine the suitability of **1** and **2** as RFB anolytes.

Table 2. Selected bond distances (Å) and angles (°) for **1** (this work) and **2**[17]

		1	**2**
Fe – N_{pyr}	Fe1 – N1	1.858(2)	1.8707(14)
	Fe1 – N4	1.860(2)	1.8655(14)
Fe – N_{imine}	Fe1 – N2	1.968(2)	1.974(2)
	Fe1 – N3	1.967(3)	1.999(2)
	Fe1 – N5	1.963(3)	1.9817(14)
	Fe1 – N6	1.966(3)	1.9922(14)
Intraligand	N1 – Fe1 – N2	79.68(10)	79.81(6)
	N1 – Fe1 – N3	80.07(10)	79.89(6)
	N2 – Fe1 – N3	159.75(10)	159.69(6)
	N4 – Fe1 – N5	80.10(10)	79.86(6)
	N4 – Fe1 – N6	80.01(11)	79.47(6)
	N5 – Fe1 – N6	160.10(10)	159.09(6)
Interligand	N1 – Fe1 – N4	179.44(11)	178.80(6)
	N1 – Fe1 – N5	100.45(10)	99.70(6)
	N1 – Fe1 – N6	99.45(10)	101.03(6)
	N2 – Fe1 – N4	100.19(11)	99.05(6)
	N3 – Fe1 – N4	100.06(11)	101.25(6)

Charge/Discharge Measurements

Battery cycling at non-dilute concentrations in an H-type cell in the absence of flow were conducted to evaluate the shelf-life stability and potential efficacy of **1** and **2** as RFB anolytes. To avoid irreversible processes, potential cut-offs were set according to a wider voltammogram (see SI, Figure S5), which revealed two irreversible reductions at more negative voltages (< -2 V vs. $FcH^{0/+}$). Setting the negative potential cut-off to potentials that allowed for a third and fourth reductive event resulted in irreversible degradation of the MCC, with the colour of the solution changing from purple to brown and formation of a precipitate. In addition, the Coulombic efficiency (%CE) of the cell decreased dramatically after 14 cycles (Figures S2 and S3). For this reason, parameters were set at a cathodic range allowing only the first and second redox couples to be accessed (Figure 2b), avoiding unwanted irreversible redox processes.

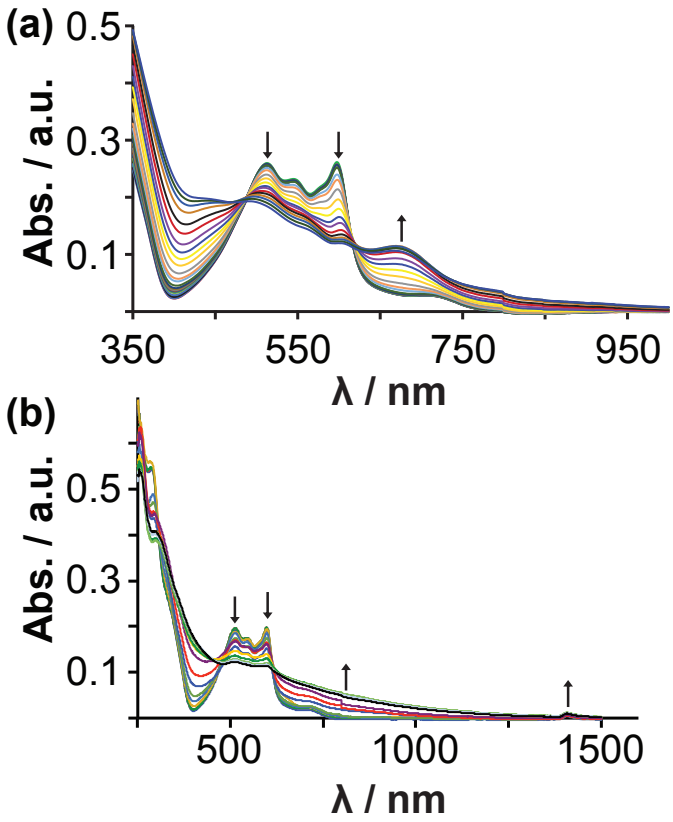

Figure 3. (a) UV-Vis spectroelectrochemistry of **1** in 0.1 M nBu$_4$NPF$_6$ acetonitrile solution, oxidative potential applied from -0.2 to 2.3 V; (b) reductive potential applied from -0.2 to -1.4 V.

Charge/discharge measurements were performed with MCCs **1** and **2** at charging rates of 0.5, 1, and 2 C. A charging rate of 1 C corresponds to a charge/discharge cycle of approximately 1 h, assuming that both 1e- reduction processes are being accessed during the electrolysis process. Charge/discharge cycling of **1** and **2** at 1 C (1.1 mA) are shown in Figure 4. During the charging segment of **1**, two plateaus corresponding to the two redox couples seen by CV/DPV (Figure 2b) are observed at -1.57 V and -1.78 V vs. $FcH^{0/+}$. Similarly for **2**, the potential was found to plateau at -1.53 V and -1.79 V vs. $FcH^{0/+}$, again agreeing with the results in Figure 2b. After extended cycling, only one clear reduction plateau at ca. -1.73 V could be observed, with a corresponding oxidation plateau at -1.36 V.

In the discharge segment, two plateaus are again observed for **1** (-0.75 and -1.51 V). While they decrease in prominence after extended cycling, the number of electrons passed per molecule remains high (~ 1.6; Figure 5a). For **2**, plateaus were observed at -1.49 and -0.91 V vs. $FcH^{0/+}$, but also fade away after two cycles. While both compounds were able to perform the full 25 cycles, the time required for **1** was slightly longer (49 hrs compared to 42 hrs) with retention of both reduction events, indicative of the higher stability of **1** to electrochemical cycling.

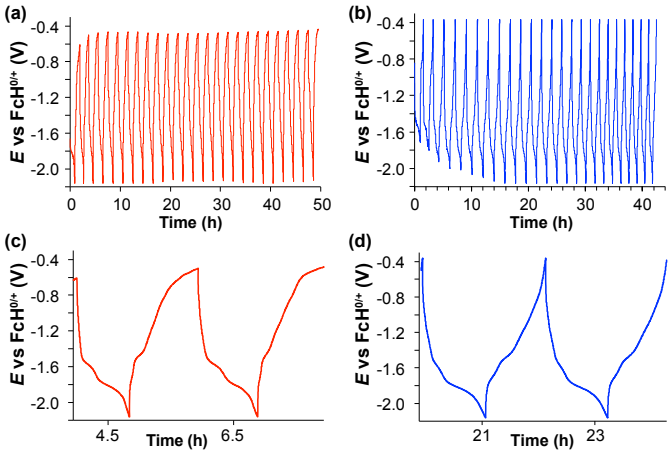

Figure 4. Total cell voltage for (a, c) **1** and (b, d) **2**. Both traces with 1.1 mA cathodic/anodic current, charging rate of 1 C and voltage limits set according to previously obtained CVs in order to limit access of irreversible redox events; in 0.4 M nBu$_4$PF$_6$ acetonitrile solution.

The long-term stability of RFB electrolytes is critical to their application. No decrease in charge capacity was observed for **1** over extended charge/discharge cycles (Figure 5), where the number of electrons stored per molecule of **1** is ca. 1.6, close to the expected value of 2. For **2**, the charge capacity was found to drop from 1.6 electrons to 1 electron over 25 cycles (Figure 5b), suggesting that only one redox event is being accessed in later cycles. Quantifying the ratio of the charge passed in charging/discharging cycles (Coulombic Efficiency, %CE) for **1** and **2** shows that **1** acts as a reversible anolyte with a high %CE of 99.9(4)% over cycles 5-25. While a reduction in capacity was observed over time, **2** showed a stable but high %CE of 94(1)% for cycles 4-25. The performance of **2** is in line with a related two electron anolyte candidate, *tris*(bpy)iron tetrafluoroborate (bpy = bipyridine), for which a decrease in capacitance from two electrons to one electron is similarly observed after 25 cycles,[5] while **1** outperforms the bpy analog in terms of stability. While **1** and **2** show less stable discharge capacities compared with MCC anolytes based on octahedral Fe^{2+} complexes of monoanionic bipyridylimino isoindoline (BPI) ligands,[6b] the cationic nature of **1** and **2** does enable their application in common ion exchange RFBs.[5]

The lower capacitance exhibited by **2** could be due to a lower solubility of the reduced form of **2**, though appreciable solid did not accumulate during battery cycling. Another possible explanation could originate in the slightly wider peak-to-peak separation (75 mV) observed by CV for the second cathodic redox couple of **2** (Table 1). While still close to the Nernstian limit of 59 mV expected for a diffusion-controlled process,[21] the wider separation implies a lower level of electrochemical reversibility, which could over time lead to a decrease in capacitance for **2** compared with **1**. Optimal ligand substitution may thus help stabilize the reversibility of the redox couples of DIP MCCs, and increase capacitance in RFB applications.

Despite **1** demonstrating a higher capacitance relative to **2**, the average number of electrons transferred (ca. 1.6) is still below the value of two expected from CV measurements due to the potential window utilized, which was selected to avoid irreversible reduction events. As the potential window was reached for these compounds at 1 C, the complexes were run at a lower charge rate (0.5 C) to determine if the full 2e$^-$ capacity could be attained. Instead, a lower capacitance is observed over cycling, with 0.71 and 0.4 electrons passed for **1** and **2** respectively (Figure S9). Similar to the %CE at 1 C, the %CE at 0.5 C was found to reside around 90(4)% for **1**, with a larger cycle-to-cycle variance observed for **2** [%CE, 89(10), see Supporting Information].

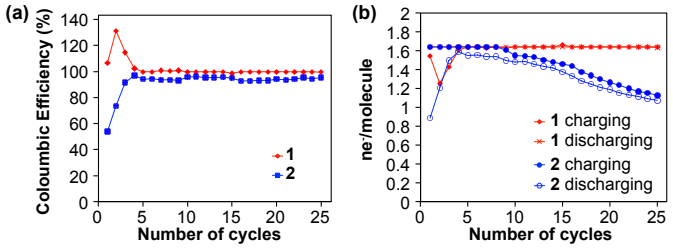

Figure 5. (a) Coulombic efficiency (%CE) for **1** and **2** at a 1 C charging rate; (b) Capacity retention for **1** and **2** at 1 C charging rate.

Electrochemical decomposition appears unlikely due to the reversibility observed both on the CV and electrolysis timescale (%CE plots), with similar number of electrons being passed during charge/discharge cycles. Precipitation or surface adsorption of the reduced species could reduce the reversibility of the redox processes, and is the likely cause of the reduced capacitance. Furthermore, at the lower charging rate employed, crossover of the reduced species to the anode is more likely the cause for decrease in capacity of both **1** and **2**, given the longer period required for each cycle. Overall, **1** presented higher %CE, number of electrons, capacitance and stability relative to **2** under the charge rates employed which we attribute to the solubilizing nature of the *t*Bu substituents of the DIP aryl substituents.

The majority of Fe-based complexes utilized in RFBs have employed ferrocene-based salts,[11] which exhibit highly reversible Fe^{3+}/Fe^{2+} redox couples that can be accessed with a high retention of capacity observed. In these complexes, the redox activity is restricted to the metal ion, with a maximum of 1e$^-$ accessible per molecule. A few reports have investigated the use of Fe-complexes with non-innocent redox ligands. Such complexes can exhibit reversible reduction character enabling use as anolytes, and more than one equivalent of electron per molecule might be accessed.[5, 6b, 15b] The anolyte candidate $[Fe(bpy)_3]^{2+}$ exhibits four redox events, but is only moderately soluble in acetonitrile and its capacity diminishes relatively quickly compared to **1** or **2**.[5, 15b] Given the ability to easily derivatize DIP ligand frameworks, the electronic and solubility properties of the metal complexes can be altered to ensure high reversibility and solubility in the solvents used and limit crossover or precipitation.

Conclusions

This work describes the utility of base metal coordination complexes supported by the well-known redox-active diimine-

pyridine (DIP) ligand scaffold in redox-flow battery applications. The high solubility, reversible electrochemistry and multi-electron storage capability of the ligand and metal make these MCCs interesting candidates as RFB anolytes and catholytes. Charge/discharge experiments exhibited multiple potential plateaus at redox potentials observed through cyclic voltammetry analysis of the complexes, and illustrate the accessibility of multiple ligand-based redox events on the bulk electrolysis (RFB) timescale. The total number of electrons stored in these solutions (1.6), however, is still below the theoretical number of reductions these complexes can undergo reversibly (2), suggesting room for optimization based on ligand substitution. The stability of these MCCs in RFB cycling and overall number of electrons transferred is also dependent on the substitution pattern of the ligand backbone, implying that the system can be engineered for greater cycling stability by addressing solubility of both species in the redox pair.[6b, 22] Future work will focus on balancing the solubility of both reduced and oxidized species, and investigate the impact of issues such as possible spin-state change upon $2e^-$ reduction of $[bis(DIP)_2Fe]^{2+}$ dications,[16] along with the overall ability of these DIP metal complexes to accommodate multiple electrons.

Experimental Section

Unless otherwise specified, all air sensitive manipulations were carried out either in a N_2 filled glove box or using standard Schlenk techniques under Ar. Proligand **L2** was prepared according to a literature procedure.[23] $FeCl_2$ (Acros), $NaPF_6$ (Alfa Aesar), $NaBPh_4$ (Sigma-Aldrich), and nBu$_4$NPF$_6$ (electrochemical grade, Sigma-Aldrich) were purchased and used without further purification. Organic solvents were dried and distilled using appropriate drying agents prior to use. 1- and 2D NMR spectra were recorded on Bruker Avance 300 MHz or Bruker Avance-III 500 MHz spectrometers. ^{1}H and ^{13}C{^{1}H} NMR spectra were referenced to residual solvent peaks. Electronic absorption spectra were recorded on an Agilent Technologies Cary 5000 Series UV-Vis-NIR spectrophotometer in dual beam mode (range: 230 – 1600 nm). Mössbauer experiments were performed in transmission geometry with a ^{57}Co in Rh source and a WissEl constant acceleration drive. Spectra were collected at 10 K using a Janis SHI-850 closed-cycle refrigerator and are calibrated relative to α-Fe at room temperature.

Synthesis of proligand L1: A 100 mL Schlenk flask was charged with 2,6-diacetylpyridine (1.11 g, 6.80 mmol) and dissolved in dry dichloromethane (20 mL). To this solution, Na_2SO_4 (1.94 g, 13.6 mmol) was added. 4-*tert*-Butylanline (3.04 mL. 19.1 mmol) was added via syringe to the solution as well as 2 drops of formic acid. The solution was allowed to stir for 48 h at room temperature. The solvent was then removed and the residue redissolved in toluene and washed with a saturated solution of Na_2CO_3 (3 x 50 mL). The organic fraction was dried over Na_2SO_4 and filtered. The solvent was removed and the solid was stirred in cold ethanol (100 mL) and then filtered. Isolated yield: 2.30 g (79 %). The NMR matches the reported literature.[23]

Synthesis of 1: A 100 mL Schlenk flask was charged with $FeCl_2$ (0.022 g, 0.18 mmol) and **L1** (0.15 g, 0.35 mmol) under N_2. Degassed MeOH (30 mL) was added and the solution immediately turned dark purple. The reaction mixture was allowed to stir for 30 min at 22 °C. Solid $NaBPh_4$ (0.18 g, 0.53 mmol) was then added and the mixture stirred for an additional 30 min. The solvent was then removed and the purple solid dissolved in CH_2Cl_2 and filtered over Celite. The filtrate was concentrated and pentane added (100 mL) to precipitate the product as a purple solid. Isolated yield: 0.281 g (90%). ^{1}H NMR (CD_3CN, 300 MHz, 25°C): δ 7.96 (m, 6H, C_{Ar}-*H*), 7.30 (ddd, 20H, J_{HH} = 8.0, 5.2, 2.5 Hz, [BPh_4] C_{Ar}-*H*), 7.19 – 7.14 (m, 8H, C_{Ar}-*H*), 6.99 (t, 20H, J_{HH} = 7.4 Hz, [BPh_4] C_{Ar}-*H*), 6.89 – 6.82 (m, 8H, C_{Ar}-*H*), 6.12 – 6.04 (m, 8H, C_{Ar}-*H*), 2.50 (s, 12H, C*H*$_3$), 1.21 ppm (s, 36H, *t*Bu). ^{13}C{^{1}H} NMR (CD_3CN, 75 MHz, 25°C): δ 178.8 (*C*=N), 165.8 – 163.8 (q, 1:1:1:1, J_{CB} = 49 Hz, C_{Ar}-B), 160.1 (CAr), 152.2 (C_{Ar}), 141.8 (C_{Ar}), 136.8 (C_{Ar}), 136.5 (C_{Ar}), 127.4 (C_{Ar}), 127.3 (C_{Ar}), 126.6 (dd, J_{CB} = 5.6, 2.7 Hz, C_{Ar}), 122.8 (C_{Ar}), 119.7 (C_{Ar}), 35.2 (*C*(CH$_3$)$_3$), 31.3 (C(*C*H$_3$)$_3$), 19.4 ppm (*C*H$_3$). Anal. Calcd for $C_{106}H_{110}B_2N_6Fe_1$: C, 82.38; H, 7.17. Found: C, 82.20; H, 7.16. Complex **1** was synthesized with hexafluorophosphate counterion for battery tests: synthetic procedure as above using $FeCl_2$ (0.030 g, 0.23 mmol), **L1** (0.2 g, 0.5 mmol) and $NaPF_6$ (0.118 g, 0.70 mmol). Isolated yield: 0.281 g (94 %). ^{1}H NMR (CD_3CN, 300 MHz, 25 °C): δ 8.05 (s, 3H, C_{Ar}-*H*), 7.17 (d, 4 H, J_{HH} = 8.7 Hz, C_{Ar}-*H*), 6.11 (d, 4 H, J_{HH} = 8.7 Hz, C_{Ar}-*H*), 2.58 (s, 6 H, CH_3), 1.19 ppm (s, 18 H, *t*Bu). ^{13}C{^{1}H} NMR (CD_3CN, 75 MHz, 25 °C): δ 178.8 (*C*=N), 160.2 (C_{Ar}), 152.1 (C_{Ar}), 141.8 (C_{Ar}), 136.5 (C_{Ar}), 127.4 (C_{Ar}), 119.7 (CAr), 35.2 (*C*(CH$_3$)$_3$), 31.3 (C(*C*H$_3$)$_3$), 19.3 ppm (*C*H$_3$). UV-Vis (CH_3CN): λ (ε) 287 (25 190), 339 (sh), 513 (8 100), 545 (7 140), 598 nm (8 310 M^{-1} cm^{-1}).

Synthesis of 2: Complex **2** has been previously published.[17] Here, **2** was prepared using an identical procedure to **1** using $FeCl_2$ (0.025 g, 0.20 mmol), **L2** (0.15 g, 0.40 mmol) and $NaPF_6$ (0.101 g, 0.60 mmol). Isolated yield: 0.199 g (91 %). Additional solution characterization data: ^{1}H NMR (CD_3CN, 300 MHz, 25 °C): δ 8.15 (s, 3H, C_{Ar}-*H*), 6.67 (d, 4 H, J_{HH} = 8.9 Hz, C_{Ar}-*H*), 6.10 (d, 4 H, J_{HH} = 8.9 Hz, C_{Ar}-*H*), 3.69 (s, 6 H, OC*H*$_3$), 2.56 ppm (s, 6 H, C*H*$_3$). ^{13}C{^{1}H} NMR (CD_3CN, 75 MHz, 25 °C): δ 179.24 (*C*=N), 160.34 (C_{Ar}), 159.80 (C_{Ar}), 137.77 (C_{Ar}), 136.62 (C_{Ar}), 127.76 (C_{Ar}), 121.83 (C_{Ar}), 115.65 (C_{Ar}), 56.29 (O*C*H$_3$), 19.44 ppm (*C*H$_3$). UV-Vis (CH_3CN): λ (ε) 291 (23 930), 343 (12 050), 518 (7 400), 549 (6 690), 603 nm (7,520 M^{-1} cm^{-1}).

X-ray data collection, solution and refinement

A dark purple, multi-faceted crystal of suitable size (0.41 x 0.25 x 0.20 mm) and quality was selected from a representative sample of crystals of the same habit using an optical microscope and mounted onto a MiTiGen loop. X-ray data were obtained on a Bruker D8 QUEST ECO CMOS diffractometer (Mo sealed X-ray tube, Kα = 0.71073 Å) at 150 K. All diffractometer manipulations, including data collection,

integration and scaling were carried out using the Bruker APEX3 software suite.[24] An absorption correction was applied using SADABS.[24] The space group was determined on the basis of systematic absences and intensity statistics and the structure was solved by direct methods and refined by full-matrix least squares on F^2. The structure was solved in the orthorhombic space group $P2_1/c$ using XS[25] (incorporated in SHELXTL). No obvious missed symmetry was reported by PLATON.[26] All non-hydrogen atoms were refined with anisotropic thermal parameters. Hydrogen atoms were places in idealized positions and refined using a riding model. Two disordered solvent molecules (CH_2Cl_2) were found co-crystallized within the large unit cell (V = 6755.3(4) Å^3) and satisfactorily modelled, as was disorder in one of the *t*Bu groups. The structure was refined (weighted least squares refinement on F^2) and the final least-squares refinement converged to R_1 = 0.0668 ($I > 2\sigma(I)$, 12 260 data) and wR_2 = 0.1967 (F^2, 15 595 data, 876 parameters).

Electrochemical Methods

Acetonitrile has proven to be the most suitable solvent for electrochemical experiments, with both coordination complexes **1** and **2** being highly soluble (solubility of **1** > 0.13 M; **2** > 0.26 M). For electrochemical analysis, 10 mg of the compound investigated was dissolved in 15 mL of 0.1 M nBu$_4$PF$_6$ in acetonitrile, and purged with Ar for 20 min prior to analysis. CV experiments were performed on a CHI 760c bipotentiostat at scan rates of 50 to 800 mV s^{-1} using a freshly polished (0.05 µm alumina paste) 3 mm diameter glassy carbon (GCE) disc working electrode, a Pt wire counter electrode, and a Ag/Ag$^+$ non-aqueous quasi-reference electrode. Differential pulse voltammetry (DPV) experiments were conducted with a 5 mV increment, a 50 mV amplitude, a 0.1 s pulse width, a 0.0167 s sample width and a 0.5 s pulse period. Ferrocene (FcH) was added as an internal standard to each solution upon completion of CV/DPV experiments, allowing potentials to be referenced to the FcH$^{0/+}$ redox couple.

For battery tests, two 15 mL acetonitrile solutions were prepared, one with 2 mM **1** or **2** and 0.4 M nBu$_4$PF$_6$, and one constituted only of 0.4 M nBu$_4$PF$_6$. Battery tests were conducted in a custom-built air-tight H-cell (see SI), with the two chambers separated by a glass frit (fine porosity), and with two outputs for the working and reference electrodes in one chamber, and one output for the counter electrode in the other chamber. The solution containing **1** or **2** was placed in the working electrode chamber, with the electrolyte-only solution placed in the counter electrode chamber and the solutions stirred continuously throughout the experiments. Reticulated vitreous carbon (RVC) counter and working electrodes were used, with a non-aqueous Ag/Ag$^+$ quasi-reference electrode. Potential cutoffs, voltages at which the reversible couples start and finish, were set according to CV results. Cycling experiments were executed at a variety of anodic and cathodic currents (0.5, 1.1 and 2.2 mA) with different (dis)charge times (1800, 3600 or 7200 s), corresponding to 0.5, 1, and 2 C charging rates assuming a 2e$^-$ reduction process, to examine the stability of the MCCs for RFB applications.

Conflicts of interest

There are no conflicts to declare.

Acknowledgements

Prof. Johan van Lierop and Kelly Newman are thanked for collecting Mössbauer spectra of **1**. The Natural Sciences Engineering Research Council of Canada is gratefully acknowledged for a CGS-M Fellowship (PKG) and Discovery Grant to DEH (RGPIN-2014-03733), as are the Canadian Foundation for Innovation and Research Manitoba for an award in support of an X-ray diffractometer (CFI #32146); the Government of Manitoba for a UMGF award (JDB); and the University of Manitoba for start-up funding (DEH) and GETS support (JDB, PKG).

References

1 *(a)* P. V. Kamat, K. S. Schanze, J. M. Buriak, *ACS Energy Lett.* 2017, **2**, 1368-1369; *(b)* J. Winsberg, T. Hagemann, T. Janoschka, M. D. Hager, U. S. Schubert, *Angew. Chem., Int. Ed.* 2017, **56**, 686-711.
2 W. Wang, V. Sprenkle, *Nat. Chem.* 2016, **8**, 204-206.
3 Y. Shao, Y. Cheng, W. Duan, W. Wang, Y. Lin, Y. Wang, J. Liu, *ACS Cat.* 2015, **5**, 7288-7298.
4 G. L. Soloveichik, *Chem. Rev.* 2015, **115**, 11533-11558.
5 S. M. Laramie, J. D. Milshtein, T. M. Breault, F. R. Brushett, L. T. Thompson, *J. Power Sources* 2016, **327**, 681-692.
6 *(a)* R. M. Darling, K. G. Gallagher, J. A. Kowalski, S. Ha, F. R. Brushett, *Energy Environ. Sci.* 2014, **7**, 3459-3477; *(b)* C. S. Sevov, S. L. Fisher, L. T. Thompson, M. S. Sanford, *J. Am. Chem. Soc.* 2016, **138**, 15378-15384.
7 V. Lyaskovskyy, B. de Bruin, *ACS Cat.* 2012, **2**, 270-279.
8 *(a)* P. J. Cappillino, H. D. Pratt, III, N. S. Hudak, N. C. Tomson, T. M. Anderson, M. R. Anstey, *Adv. Energy Mater.* 2014, **4**, 1300566/1-1300566/4; *(b)* P. J. Cabrera, X. Yang, J. A. Suttil, K. L. Hawthorne, R. E. M. Brooner, M. S. Sanford, L. T. Thompson, *J. Phys. Chem. C* 2015, **119**, 15882-15889; *(c)* P. J. Cabrera, X. Yang, J. A. Suttil, R. E. M. Brooner, L. T. Thompson, M. S. Sanford, *Inorg. Chem.* 2015, **54**, 10214-10223.
9 V. C. Gibson, C. Redshaw, G. A. Solan, *Chem. Rev.* 2007, **107**, 1745-1776.
10 *(a)* D. Enright, S. Gambarotta, G. P. A. Yap, P. H. M. Budzelaar, *Angew. Chem., Int. Ed.* 2002, **41**, 3873−3876; *(b)* J. J. Kiernicki, P. E. Fanwick, S. C. Bart, *Chem. Commun.* 2014, **50**, 8189-8192; *(c)* A. M. Tondreau, S. C. E. Stieber, C. Milsmann, E. Lobkovsky, T. Weyhermüller, S. P. Semproni, P. J. Chirik, *Inorg. Chem.* 2013, **52**, 635-646.
11 *(a)* K. Park, J. H. Cho, K. Shanmuganathan, J. Song, J. Peng, M. Gobet, S. Greenbaum, C. J. Ellison, J. B. Goodenough, *J. Power Sources* 2014, **263**, 52-58; *(b)* Y. Zhao, Y. Ding, J. Song, G. Li, G. Dong, J. B. Goodenough, G. Yu, *Angew. Chem., Int. Ed.* 2014, **53**, 11036-11040; *(c)* B. Hwang, M.-S. Park, K. Kim, *ChemSusChem* 2015, **8**, 310-314; *(d)* X. Wei, L. Cosimbescu, W. Xu, J. Z. Hu, M. Vijayakumar, J. Feng, M. Y. Hu, X. Deng, J. Xiao, J. Liu, V. Sprenkle, W. Wang, *Adv. Energy Mater.* 2015, **5**, 1400678/1-1400678/7; *(e)* E. S. Beh, D. De Porcellinis, R. L. Gracia, K. T. Xia, R. G. Gordon, M. J. Aziz, *ACS Energy Lett.*

2017, **2**, 639-644; *(f)* G. Cong, Y. Zhou, Z. Li, Y.-C. Lu, *ACS Energy Lett.* 2017, **2**, 869-875; *(g)* B. Hu, C. DeBruler, Z. Rhodes, T. L. Liu, *J. Am. Chem. Soc.* 2017, **139**, 1207-1214.
12 *(a)* K. Gong, F. Xu, J. B. Grunewald, X. Ma, Y. Zhao, S. Gu, Y. Yan, *ACS Energy Lett.* 2016, **1**, 89-93; *(b)* M. O. Bamgbopa, Y. Shao-Horn, S. Almheiri, *J. Mater. Chem. A* 2017, **5**, 13457-13468.
13 *(a)* J. Mun, M.-J. Lee, J.-W. Park, D.-J. Oh, D.-Y. Lee, S.-G. Doo, *Electrochem. Solid-State Lett.* 2012, **15**, A80-A82; *(b)* T. M. Anderson, M. Anstey, N. C. Tomson, Sandia Corporation, 2014, US20140239906A1.
14 W. Kaim, *Eur. J. Inorg. Chem.* 2012, 343-348.
15 *(a)* Y. Matsuda, K. Tanaka, M. Okada, Y. Takasu, M. Morita, T. Matsumura-Inoue, *J. Appl. Electrochem.* 1988, **18**, 909-914; *(b)* M. H. Chakrabarti, R. A. W. Dryfe, E. P. L. Roberts, *Electrochim. Acta* 2006, **52**, 2189-2195; *(c)* M.-S. Park, N.-J. Lee, S.-W. Lee, K. J. Kim, D.-J. Oh, Y.-J. Kim, *ACS Appl. Mater. Interf.* 2014, **6**, 10729-10735; *(d)* D. M. Cabral, P. C. Howlett, D. R. MacFarlane, *Electrochim. Acta* 2016, **220**, 347-353.
16 B. M. Wile, R. J. Trovitch, S. C. Bart, A. M. Tondreau, E. Lobkovsky, C. Milsmann, E. Bill, K. Wieghardt, P. J. Chirik, *Inorg. Chem*., 2009, **48**, 4190-4200.
17 B. De Bruin, E. Bill, E. Bothe, T. Weyhermueller, K. Wieghardt, *Inorg. Chem.*, 2000, **39**, 2936-2947.
18 J. M. Darmon, S. C. E. Stieber, K. T. Sylvester, I. Fernandez, E. Lobkovsky, S. P. Semproni, E. Bill, K. Wieghardt, S. DeBeer, P. J. Chirik, *J. Am. Chem. Soc.*, 2012, **134**, 17125-17137.
19 D. L. Sun, S. V. Rosokha, S. V. Lindeman and J. K. Kochi, *J. Am. Chem. Soc.*, 2003, **125**, 15950-15963.
20 J. Noack, N. Roznyatovskaya, T. Herr, P. Fischer, *Angew. Chem., Int. Ed.*, 2015, **54**, 9776-9809.
21 A. J. Bard, L. R. Faulkner, *Electrochemical Methods: Fundamentals and Applications*, John Wiley and Sons, Inc., Hoboken, 2001.
22 C. S. Sevov, R. E. M. Brooner, E. Chénard, R. S. Assary, J. S. Moore, J. Rodríguez-López, M. S. Sanford, *J. Am. Chem. Soc.*, 2015, **137**, 14465-14472.
23 B. Cetinkaya, E. Cetinkaya, M. Brookhart, P. S. White, *J. Mol. Catal. A: Chem.*, 1999, **142**, 101-112.
24 Bruker-AXS, Madison, Wisconsin, USA, 2016.
25 G. M. Sheldrick, *Acta Cryst.*, 2008, **A64**, 112-122.
26 A. L. Spek, *Acta Cryst.*, 2009, **D65**, 148-155.